ROYAL SOCIETY
OF CHEMISTRY

REVIEW

CrossMark
click for updates

Thermodynamics and structure of macromolecules from flat-histogram Monte Carlo simulations†

Wolfhard Janke*[a] and Wolfgang Paul*[b]

Over the last decade flat-histogram Monte Carlo simulations, especially multi-canonical and Wang–Landau simulations, have emerged as a strong tool to study the statistical mechanics of polymer chains. These investigations have focused on coarse-grained models of polymers on the lattice and in the continuum. Phase diagrams of chains in bulk as well as chains attached to surfaces were studied, for homopolymers as well as for protein-like models. Also, aggregation behavior in solution of these models has been investigated. We will present here the theoretical background for these simulations, explain the algorithms used and discuss their performance and give an overview over the systems studied with these methods in the literature, where we will limit ourselves to studies of coarse-grained model systems. Implementations of these algorithms on parallel computers will be also briefly described. In parallel to the development of these simulation methods, the power of a micro-canonical analysis of such simulations has been recognized, and we present the current state of the art in applying the micro-canonical analysis to phase transitions in nanoscopic polymer systems.

1 Introduction

In the past few decades computer simulation studies have become an increasingly important numerical tool for the study and understanding of polymeric systems. Two main approaches can be distinguished. Molecular dynamics (MD) simulations[1–3] are based on numerical integration of Newton's equation of motion of the system and deliver information on its thermodynamics, structure

[a] *Institut für Theoretische Physik, Universität Leipzig, 04009 Leipzig, Germany.*
E-mail: Wolfhard.Janke@itp.uni-leipzig.de
[b] *Institut für Physik, Martin-Luther-Universität, 06099 Halle, Germany.*
E-mail: Wolfgang.Paul@physik.uni-halle.de
† Dedicated to Thomas Neuhaus who unexpectedly passed away on 1 June 2015.

Wolfhard Janke received his PhD in physics in 1985 from the Free University Berlin, Germany. After postdoctoral stays at Florida State University, USA, and Forschungszentrum Jülich, Germany, he spent a Heisenberg Professorship at Mainz University in Prof. Kurt Binder's group. Since 1998 he has been Full Professor for Computer-oriented Quantum Field Theory at the University of Leipzig, Germany. He is an ''International Visiting Professor'' of Coventry University, England, and since 2015 has been Adjunct Professor of University of Georgia, USA. His research interests focus on the statistical physics of polymers, phase transitions and critical phenomena, materials with quenched, random disorder, and low-dimensional quantum spin systems.

Wolfhard Janke

Wolfgang Paul received his PhD in physics in 1989 from Johannes Gutenberg University in Mainz, Germany, working with Prof. Kurt Binder. After his PhD he started to work on polymer physics problems and spent a postdoctoral time at the IBM Almaden research center in San Jose, USA. He received his habilitation in 1997 from Johannes Gutenberg University where he became Associate Professor in 2003. Since 2009 he has been Full Professor for Theoretical Polymer Physics at Martin Luther University in Halle, Germany. His research covers thermodynamcis, the structure and dynamics of polymer Systems, as well as applications of stochastic processes in physics.

Wolfgang Paul

and dynamics. Monte Carlo (MC) methods[2,4–7] rely on the stochastic ensemble formulation of the statistical physics of the polymer model. They are mainly geared towards providing thermodynamic and structural information but can be formulated to study relaxation behavior as well. Depending on the application at hand and the degree of chemically realistic modeling both approaches may directly be compared with experiments or support analytical theory by yielding accurate data for assessment of the usually necessarily employed approximations. In this sense, computer simulations have become the third cornerstone of modern polymer science beyond experiments and analytical theory. The great success of computer simulations depends in part on the constant improvements of the computer hardware, but in particular MC simulations have even more profited from considerable methodological developments. Among them are the very successful flat-histogram MC techniques which are in the focus of the present mini review.

To understand the importance of flat-histogram simulation techniques, let us contrast them with the more standard importance sampling MC methods and their most prominent representative, canonical MC simulations. In the canonical ensemble of statistical mechanics, defined by fixing the macroscopic variables particle number, N, volume, V, and temperature, T, every micro-state, x, occurs with the probability

$$p_{eq}(x) = \frac{1}{Z(N,V,T)} e^{-\beta U(x)}, \tag{1}$$

where $\beta = 1/k_B T$ is the inverse temperature and $U(x)$ the potential energy of the system, assumed to depend only on the configuration variable x. The normalization factor is given by the canonical partition function

$$Z(N,V,T) = \int_\Gamma dx\, e^{-\beta U(x)}, \tag{2}$$

with Γ denoting the configuration space of the system. Already for mesoscopic systems occurring in a simulation, the Boltzmann factor $e^{-\beta U(x)}$ is sharply peaked at the minima of the potential energy. The efficient determination of the thermodynamic average of an observable $A(x)$ given by

$$\langle A \rangle = \int_\Gamma dx\, A(x) p_{eq}(x) \tag{3}$$

therefore requires any discretization of this high-dimensional integral to include the points where the Boltzmann factor contributes the most. This is achieved, when one generates the sampling points of the integral discretization through a Markov chain MC method

$$p(x, n+1) = p(x,n) + \int_\Gamma dx'\, W(x|x') p(x',n) \\ - \int_\Gamma dx'\, W(x'|x) p(x,n) \tag{4}$$

with transition densities $W(x|x')$ for going from state x' at discrete time n to x at time $n+1$. The general mathematical theory of such Markov chains yields criteria for their convergence to a unique equilibrium distribution; in the physics

literature the most common practice is to use the detailed balance condition

$$\frac{W(x|x')}{W(x'|x)} = \frac{p_{eq}(x)}{p_{eq}(x')} = e^{-\beta[U(x)-U(x')]}. \tag{5}$$

The fact that the unknown partition function drops out of this equation is the basis for the success of the canonical MC method, but at the same time it delineates its limitations. The method as such is not able to determine entropies or free energies from the simulation, as these would need knowledge of the density of states, $g(N,V,E)$, of the model, which is the micro-canonical partition function from which the canonical one is obtained by Laplace transform,

$$Z(N,V,T) = \int dE\, g(N,V,E) e^{-\beta E}. \tag{6}$$

Within the scope of MC this shortcoming is most successfully addressed by two flat-histogram MC schemes, the multi-canonical MC (MuMC) and the Wang–Landau MC (WLMC) scheme and its mathematical pendant, stochastic approximation MC (SAMC). Both schemes aim at sampling the macroscopic variable energy with a uniform probability distribution and achieve this by related, but somewhat different means. They are developments out of the classic idea of umbrella sampling MC[8] and can be formulated for the uniform sampling of other macroscopic variables as well. In the literature, there exist reviews on the MuMC method[6,9–11] and the Wang–Landau method,[12–15] so we will focus here especially on their application to the thermodynamics and structure of polymer systems. Also, for the WLMC method some mathematical background relating it to the SAMC approach needs to be reviewed.

In the following sections we will first present the mathematical background on MuMC, WLMC and SAMC, and then turn to selected results obtained with these methods for the thermodynamics and structure of polymer systems. A final section will present our conclusions and an outlook.

2 Background on the simulation methods

This section will present the idea and the background on the MuMC and the WLMC and SAMC algorithms and discuss some particulars of their application to polymer systems.

2.1 Multi-canonical Monte Carlo

The idea of multi-canonical MC (MuMC or "muca") methods dates back to 1991/92 when Berg and Neuhaus[16,17] proposed a novel simulation approach for overcoming the exponential (sometimes called "super-critical") slowing down of MC simulations at first-order phase transitions in the canonical ensemble. For finite systems, the phase coexistence at (temperature driven) first-order phase transitions is reflected by a double peak of the energy distribution $P_{can,\beta}(E)$, with the minimum in between governed by the (reduced) interface tension σ_{od} between the coexisting ordered and disordered phases: $P_{min}/P_{max} \propto \exp(-2\sigma_{od}L^{d-1})$, where L is the linear size of a d-dimensional

cubic system and periodic boundary conditions are assumed. Due to this exponential suppression with increasing system size, it is very unlikely to transit in a canonical simulation from one phase to the other and hence it is very time consuming to generate accurate equilibrium results.

By "filling" this rare-event region with an artificial weight factor $W(E)$ (to be determined below), their method may be viewed as a specific realization of non-Boltzmann sampling which has been known since long as a legitimate alternative to the more standard MC approaches.[18] In this interpretation, the multi-canonical method appears as a non-standard reweighting approach,[19] a view which in most cases simplifies the actual implementation and paves the way to multidimensional generalizations. Alternatively, their method may be interpreted as a suitable combination of canonical statistics over an extended temperature or energy range in a single simulation run, instead of patching many independent canonical simulations at different temperatures as in (static) reweighting procedures such as the weighted histogram analysis method (WHAM).[20,21] The latter view is stressed in the original papers by Berg and Neuhaus[16,17] and explains the name "*multi*-canonical".

It should be noted that the practical significance of non-Boltzmann sampling has, in fact, already been demonstrated much earlier by Torrie and Valleau[8] with the "umbrella sampling" method. Most of these early applications aimed at reliable computations of free-energy differences which can be obtained by canonical Boltzmann sampling only indirectly *via* so-called thermodynamic integration. Later the attention slowly shifted to problems with rare-event sampling and quasi-ergodicity,[22] but it took many years before the development of the multi-canonical scheme turned non-Boltzmann sampling into a widely appreciated practical tool in computer simulation studies. Once the feasibility of such generalized ensemble approach was realized, it was for instance readily introduced into protein folding studies[11,23] and many related methods were developed.

The multi-canonical method may be viewed as a two-step process, where one first iteratively improves guesses of an *a priori* unknown weight function $W(E)$ for (*e.g.*, polymer) configurations x with system energy $E(x)$ which replaces the usual Boltzmann weight $e^{-\beta E}$ in the canonical partition function (2) and (6):

$$Z(T) = \sum_x e^{-\beta E(x)} = \sum_E g(E) e^{-\beta E}$$
$$\rightarrow Z_{MuMC} = \sum_x W(E(x)) = \sum_E g(E) W(E). \quad (7)$$

Here and in the following we omit the arguments N, V of the canonical partition function and the density of states. Correspondingly, the acceptance criterion of traditional Metropolis MC simulations is modified to

$$p_{acc}(x \rightarrow x') = \min\left(1, e^{-\beta(E'-E)}\right)$$
$$\rightarrow \min\left(1, \frac{W(E')}{W(E)}\right), \quad (8)$$

where $E \equiv E_{old}$ is the current or "old" energy of the configuration (or micro-state) x and $E' \equiv E_{new}$ the "new" energy of a proposed

updated configuration x'. As in Metropolis simulations, the update proposals for going from a configuration x to a configuration x' may be local (such as end rotation, bend, or crankshaft moves for polymers) or non-local (such as spherical rotation or pivot moves).

After having determined an accurate multi-canonical weight $W(E)$, this is kept fixed and following some thermalization sweeps a long production run is performed, where any statistical quantity O can be "measured" multi-canonically,

$$\langle O \rangle_{MuMC} = \sum_x O(x) W(E(x))/Z_{MuMC}. \quad (9)$$

The usually desired canonical statistics can be obtained by reweighting the multi-canonical to the canonical distribution, *e.g.*, canonical expectation values (3) are computed as

$$\langle O \rangle(\beta) = \langle O e^{-\beta E} W(E)^{-1} \rangle_{MuMC} / \langle e^{-\beta E} W(E)^{-1} \rangle_{MuMC}. \quad (10)$$

Note that this representation is exact for any choice of $W(E)$. As usual, in a simulation run with N measurements, the expectation values are replaced by mean values (their "estimators"), *e.g.*, $\langle O \rangle(\beta) = \langle O e^{-\beta E} W(E)^{-1} \rangle_{MuMC} / \langle e^{-\beta E} W(E)^{-1} \rangle_{MuMC} \approx \sum_{i=1}^{N} O_i e^{-\beta E_i} W(E_i)^{-1} / \sum_{i=1}^{N} e^{-\beta E_i} W(E_i)^{-1}$. Of course, the ratio of expectation values on the right-hand side of (10) is in principle prone to bias effects, but here strong cross-correlations act positively and keep this potential problem small.

The key of the multi-canonical method lies in the first step where the weight $W(E)$ is usually adjusted in such a way that the transition probabilities between configurations with different energies become roughly constant, giving an approximately flat energy histogram

$$H(E) \propto P_{MuMC}(E) = g(E) W(E) \approx \text{const.} \quad (11)$$

If this can be achieved, the simulation thus performs approximately a random walk through energy space. The second step is the actual production run, which works with fixed weights as produced iteratively in step one. By this one assures that detailed balance is implemented in the same way as in the standard Metropolis Markov chain procedure.

The formal solution of (11) is $W(E) = g^{-1}(E)$. However, since the density of states $g(E)$ is usually not known beforehand one has to proceed by a weight iteration which is initialized by setting $W(E) = W^{(0)}(E) \equiv 1$. One thus performs a standard canonical simulation at $\beta = 0$ which yields $H^{(0)}(E) \propto P_{can,\beta=0}(E)$. This current multi-canonical histogram is used to determine the next guess for the weights, the simplest update is to calculate $W^{(1)}(E) = W^{(0)}(E)/H^{(0)}(E)$. The following run is performed with $W^{(1)}(E)$ inserted in (7) and (8), which gives the energy histogram $H^{(1)}(E)$ and an improved estimate of the weight function, $W^{(2)}(E) = W^{(1)}(E)/H^{(1)}(E)$. This iterative procedure can be continued,

$$W^{(n+1)}(E) = W^{(n)}(E)/H^{(n)}(E), \quad (12)$$

until the multi-canonical histogram $H^{(n)}(E)$ is judged to be "flat" enough. From (12) it is obvious that once $H^{(n)}(E) \approx$ const,
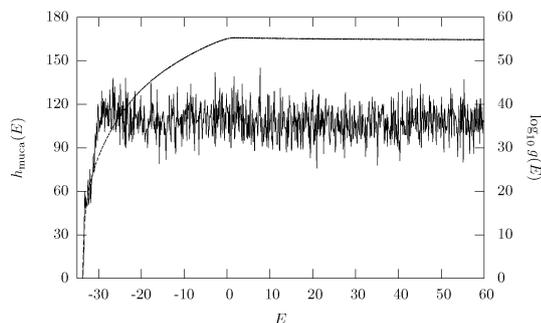
Fig. 1 The almost horizontal line fluctuating between 90–120 counts per energy bin shows the flat multi-canonical energy histogram $h_{\mathrm{muca}}(E)$ and the smooth curve spanning about 50 orders of magnitude depicts the resulting density of states $g(E)$. The data are obtained from a MuMC simulation of an AB heteropolymer with 20 monomers forming the sequence $BA_6BA_4BA_2BA_2B_2$ (taken from ref. 24).

$W^{(n+1)}(E) \propto W^{(n)}(E) \propto g^{-1}(E)$ is at a fixed point of the iteration and will not change anymore.

An example for an AB heteropolymer chain[24] is shown in Fig. 1. Here the density of states $g(E)$ varies over about 50 orders of magnitude. This sounds already like a lot, but once the multi-canonical iteration is set up, it can be driven even much further: Fig. 3 of ref. 25 and Fig. 2 of ref. 26 show density of states that are covering more than 3000 orders of magnitude (for a 309-mer)!

An important parameter of this procedure is the simulation length $N^{(n)}$ in the nth iteration step. If this is too small, the resulting multi-canonical histogram is very noisy, which enters directly in the generalized Boltzmann probabilities of the next iteration step. On the other hand, in order to optimize the total time needed to construct the final multi-canonical weight, $N^{(n)}$ should also not chosen to be too large. Since here also auto-correlation times (in the intermediate multi-canonical ensembles during the iteration) play an important role, it is not straight-forward to give an *a priori* estimate of the optimal values of $N^{(n)}$ (which, in fact, may vary with the iteration level n).

Another option to tune the performance of the weight iteration is choosing a suitable energy range, in which the "flattening" of the multi-canonical distribution is started, for the problem at hand. For instance, for a temperature driven first-order phase transition it may be useful to place this range in the regime between the two peaks of $P_{\mathrm{can},\beta}(E)$ associated with the disordered and ordered phases. This can be simply achieved by setting initially $W^{(0)}(E) \equiv e^{-\beta_0 E}$ (instead of $\equiv 1$) for a suitably chosen β_0. This corresponds to a canonical simulation at $\beta = \beta_0$ in the 0th iteration step, resulting in $H^{(0)}(E) \propto P_{\mathrm{can},\beta_0}(E)$ which covers the desired energy range around $\langle E \rangle(\beta_0)$. The remaining iteration then proceeds as before.

An efficient construction of the weight $W(E)$ is the most important technical part of multi-canonical simulations. As outlined above, the caveat of the simple direct iteration scheme is its sensitivity to the run times $N^{(n)}$. A more sophisticated recursion, in which the new weight factor is computed from all available data accumulated so far, reduces this dependency significantly and as a consequence is more robust. Noting that in the Metropolis acceptance criterion (8) only weight ratios

enter, it is useful to define $R(E) = W(E + \Delta E)/W(E)$ with some ΔE. The accumulative weight iteration then works as follows:

(1) Perform a simulation with $R^{(n)}(E)$ to obtain the histogram $H^{(n)}(E)$, taking $N^{(n)}$ energy measurements.

(2) Compute the statistical weight of the nth run:

$$p(E) = H^{(n)}(E)H^{(n)}(E + \Delta E)/[H^{(n)}(E) + H^{(n)}(E + \Delta E)]. \quad (13)$$

(3) Accumulate statistics:

$$p^{(n+1)}(E) = p^{(n)}(E) + p(E), \quad (14)$$

$$\kappa(E) = p(E)/p^{(n+1)}(E). \quad (15)$$

(4) Update weight ratios:

$$R^{(n+1)}(E) = R^{(n)}(E)[H^{(n)}(E)/H^{(n)}(E + \Delta E)]^{\kappa(E)}. \quad (16)$$

Goto step 1.

The recursion is initialized with $p^{(0)}(E) = 0$. Due to the accumulated statistics, this procedure is rather insensitive to the length $N^{(n)}$ of the nth run in step 1. The idea behind (13) is that the *a priori* error estimate for a histogram $H(E)$ (normalized to total counts) is given by $\sqrt{H(E)}$. The rest is basically just error propagation. Of course, to arrive at handy and easy-to-use formulas some approximations are necessary, such as neglecting autocorrelation times, cross-correlations in histograms *etc.*, but apart from that the accumulative recursion has a firm theoretical basis.

Finally it should be stressed that also when employing flat-histogram ideas the choice of update proposals can play a crucial role for the success of polymer simulations.[26] Moreover, it turned out to be very useful to allow the range of the proposed update moves to become energy dependent (at high energies corresponding to high temperatures, large moves will be accepted, whereas at low energies corresponding to low temperatures, only small moves have a reasonable acceptance probability). Of course, *a priori* this energy dependence causes violations of detailed balance. This can be regained, however, by introducing suitable bias correction factors in a Metropolis–Hastings scheme.[26]

At times where the computer performance increases mainly in terms of parallel processing on multi-core architectures, it is crucial to parallelize the applied algorithm. With this in mind, Zierenberg *et al.*[27] recently developed a parallel implementation of the multi-canonical method. The parallelization relies on independent equilibrium simulations that only communicate when the multi-canonical weight function is updated. That way, the Markov chains efficiently sample the temporary distributions allowing for good estimations of consecutive weight functions. For similar approaches see ref. 28 and 29.

Overall, the parallelization was shown to scale quite well in applications to generic spin models and coarse-grained polymers.[27,30,31] In all cases, a close to linear scaling was observed with slope one for up to 128 cores used. This means that doubling the number of involved processors would reduce the wall-clock time necessary by a factor of two. It is a straight-forward and simple implementation especially if wrapped around an existing multi-canonical simulation code. Therefore the

parallelization can be easily applied also to other flat-histogram simulations, *e.g.*, multimagnetic simulations where the magnetization[32,33] or any order-parameter[34,35] distribution is flattened. It should be emphasized that no greater adjustment to the usual implementation is necessary and that additional modifications may be carried along. This allows a straightforward application of this parallelization to a broad class of complex systems such as (bio)polymers and (spin) glasses.

2.2 Wang–Landau Monte Carlo and SAMC

In 2001 F. Wang and D. P. Landau published two ground breaking papers[36,37] presenting a new simulation method aimed at determining the density of states of a model system and applied it to the 2d Ising model and other spin models, and in 2002 the first application to the phase behavior of a liquid[38] was published. The basic idea is the following. If one assumes that a given MC procedure moves through the configuration space of a system in an unbiased fashion, then the probability for the next state, x', in a Markov chain to have an energy, E', is proportional to the number of states $g(E')\Delta E$ in the interval $[E',E' + \Delta E]$. Equally, the probability to start this move from a specific micro-state, x, belonging to the energy, E, is given by $1/(g(E)\Delta E)$. When one now accepts this move with an acceptance probability proportional to the ratio of the densities of states $g(E)/g(E')$, the MC procedure should lead to a random walk over the allowed energy values of the model and thus to a uniform sampling of all energy states.

The problem here is, as in the MuMC approach, that $g(E)$ is just the unknown quantity the method aims to determine. This is realized through the following basic schematic iteration procedure:

(1) Start with the unbiased guess $g(E) = 1 \,\forall E$, a visitation histogram $H(E) = 0 \,\forall E$ and a modification factor $f = f_0$.

(2) Perform a MC move going from x to x' (*i.e.*, from E to E') and accept it with the Metropolis-like acceptance criterion $\min(1,g(E)/g(E'))$. If the move is accepted, update $g(E') = fg(E')$ and $H(E') = H(E') + 1$, else update $g(E) = fg(E)$ and $H(E) = H(E) + 1$.

(3) Check whether the visitation histogram is flat, *i.e.*, $(1 - c)\overline{H(E)} < H(E) < (1 + c)\overline{H(E)}$, where $\overline{H(E)}$ is the average visitation. If this is fulfilled set $H(E) = 0 \,\forall E$ and $f = \sqrt{f}$ and go to 2. If it is not fulfilled go to 2 directly.

(4) Stop when $f < 1 + \varepsilon$.

Typical choices are $f_0 = e$, $c = 0.2$ and $\varepsilon = 10^{-9}$. Wang and Landau showed that this scheme is empirically able to reproduce, *e.g.*, the analytically known density of states of the 2d Ising model to a very high accuracy, but why? Clearly, the schematic description of the algorithm already shows that the method is not in the class of Markov chain MC methods, as the acceptance criterion at any time depends on the history of the simulation. Zhou and Bhatt[39] argued that the WL algorithm converges, if one can assume the sub-ordinate process generated on the macroscopic variable (*i.e.*, the energy in the above discussion) to be a Markov process, but just assumed that this would be the case if the updates of the density of states are spaced in time with an interval larger than the autocorrelation

time of the underlying MC process. They also proved that the final error of the above scheme scales as $\sqrt{\ln f}^{-1}$ with a final modification factor f, which was verified in simulations.[40,41] To overcome this limitation, a modification of the original method has been suggested,[42,43] where the modification factor is changed asymptotically proportional to $1/t$ (t being the simulation time). In this method the final error is not bounded from below, however, it has been pointed out,[44] that the practical performance of this version of WLMC for polymer simulations depends on the physical model it is applied to.

In parallel to much of this development, within the mathematical literature on stochastic optimization problems Stochastic Approximation Monte Carlo (SAMC) has been formulated.[45–47] Using the mathematical background of stochastic approximation methods, Liang *et al.*[46] proved the convergence of SAMC and showed that WLMC could be seen as a version of SAMC. The starting point of SAMC is the same as for WLMC. Assume a configuration space, Γ, and a microscopic probability density, $\psi(x)$, on this space. Assume an energy interval $[E_{\min},E_{\max}]$ which can be larger than the admissible energy range of the model system, specifically one can choose $E_{\min} < E_{gs}$, where E_{gs} is the ground-state energy of the model. We further assume that we have a set of M discrete energy states, either because they are intrinsic to the model or because we have performed a numerically necessary binning of adjacent energies when the model has a continuous variation of admissible energies. This set of energies leads to a unique partitioning of the microscopic configuration space Γ,

$$g(E_i) = \int_{E_i \leq U(x) < E_i+\Delta E} \mathrm{d}x\, \psi(x). \tag{17}$$

Let $\tilde{g}(E_i,t)$ denote the approximation of $g(E_i)$ at time t in the simulation and define $S_i(t) = \ln \tilde{g}(E_i,t)$. Perform a Markov chain MC simulation with the stationary distribution

$$p(x) \propto \sum_{i=1}^{M} \frac{\psi(x)}{\tilde{g}(E_i, t)} \chi_i(x), \tag{18}$$

where $\chi_i(x) = 1$ if $E_i \leq U(x) < E_i + \Delta E$ and zero elsewhere. If a new state x' with energy E_j is generated from a state x with energy E_i with a conditional probability $q(x'|x)$ then the Metropolis acceptance criterion of this Markov chain is given as

$$\min\left(1, \frac{\tilde{g}(E_i, t)}{\tilde{g}(E_j, t)} \frac{\psi(x')}{\psi(x)} \frac{q(x'|x)}{q(x|x')}\right). \tag{19}$$

Finally, the update of the guess for the density of states is performed on its logarithm:

$$\mathbf{S}(t + 1) = \mathbf{S}(t) + \gamma_t(\mathbf{e}(t) - \mathbf{p}^\star). \tag{20}$$

The modification factor is typically chosen as $\gamma_t = \gamma_0 t_0/\max(t_0,t)$, *i.e.*, it has an asymptotic $1/t$ dependence. $\mathbf{S}$, $\mathbf{e}$, $\mathbf{p}^\star$ are M-dimensional vectors. $\mathbf{S}$ is the vector of the $\{S_i(t)\}_{i=1,\dots,M}$, the vector $\mathbf{e} = (0, 0,\dots,1, 0,\dots,0)$ has a one in the position of the energy value after the move, and the vector $\mathbf{p}^\star$ is a biasing probability which will be the

sampling frequency of the energy states when the process is converged, *i.e.*, one has

$$\sum_{E=E_{\min}}^{E_{\max}} p^*(E) = 1. \tag{21}$$

The following two necessary conditions exist for this method to converge:[45,46]

$$\sum_{t=1}^{\infty} \gamma_t = \infty, \tag{22}$$

$$\sum_{t=1}^{\infty} \gamma_t^{\nu} < \infty \text{ for some } \nu \in (1, 2). \tag{23}$$

The first of these conditions is violated by the original update version[36,37] of WLMC which explains its lack of convergence, but it is fulfilled in the modified $1/t$ update of ref. 42 and 43. The SAMC update scheme converges in the following form:

$$\ln[\tilde{g}(E)] \to \ln[g(E)] + C - \ln[p^*(E) + \Phi] \quad \text{if } E \in \{E\}_{\text{adm}}, \tag{24}$$

$$\ln[\tilde{g}(E)] \to 0 \quad \text{if } E \notin \{E\}_{\text{adm}}, \tag{25}$$

where $\{E\}_{\text{adm}}$ is the set of admissible energy values of the model and C is an undetermined constant. If we let M_0 be the number of energy states in the chosen energy interval which are not admissible energy states of the model, then

$$\Phi = \frac{1}{M - M_0} \sum_{E \notin \{E\}_{\text{adm}}} p^*(E). \tag{26}$$

The sampling frequency we introduced, $p^*(E)$, defines the visitation probability of the different energy states when the procedure converges, *i.e.*, for a converged simulation and one has

$$\frac{H(E)}{\sum_E H(E)} \to p^*(E) \quad E \in \{E\}_{\text{adm}}. \tag{27}$$

The choice of $p^*(E)$ is arbitrary, however, different choices may prove more or less efficient in sampling rare states in configuration space.

To make contact with the WLMC method we have to consider a flat sampling of configuration space, *i.e.*, $\psi(x) = \text{const}$, without biasing the moves, *i.e.*, $q(x'|x) = q(x|x')$ and a flat target sampling of the energy interval, $p^*(E) = 1/M$. Then (19) gives the acceptance rate of the WLMC scheme, and we have from (24)

$$\ln[\tilde{g}(E_i, t)] \to \ln[g(E_i)] + C' \tag{28}$$

where we have subsumed all constants on the right side into one constant C'. Since $\ln[g(E_i)]$ can only be determined up to an unknown constant anyway, this is the approximation idea of the WLMC method. A discussion of the convergence of WLMC therefore should not be performed within the context of Markov chain Monte Carlo methods and detailed balance conditions, but as a special case of SAMC.

There are, however, several algorithmic advantages in using the SAMC scheme:

• The flatness criterion in the WLMC scheme only works if the energy range or energy values of a model system are determined beforehand, whereas in SAMC one can work with an arbitrary range encompassing the physical one.

• Even then, the WLMC iteration sometimes does not stop, due to the stochastic nature of the time when the flatness criterion is reached. SAMC in contrast is stopped after a predetermined time, when γ_t drops below some chosen threshold.

• SAMC allows for a selective bias towards a chosen energy range by selecting the sampling probabilities $\mathbf{p}^*$.

The quality of convergence of SAMC, however, is determined by the same requirement as in WLMC, the final visitation histogram to the energy states has to be flat (after normalization by the bias $\mathbf{p}^*$ if necessary). The applicability of SAMC for polymer simulations has recently been analyzed in detail by Werlich *et al.*[48]

The WLMC method has been parallelized along similar ideas used in the parallelization of the MuMC method[49] and tested on applications to, *e.g.*, spin systems and adsorption of polymers onto walls. The scheme consisted of parallel threads calculating the density of states in overlapping energy intervals partitioning the complete energy range, which could be exchanged when they reached the same energy value. The performance of this parallel approach, as usual, sensitively depended on the choice of simulation parameters.

3 Selected results

In this section we will present selected results achieved by the application of MuMC and WLMC approaches to polymer physics problems. The presentation will be along the physical problems and not the methods as in the previous section. We will focus on results we find of general relevance and will strive for a covering of what we find to be the essential literature in the area. We will furthermore limit our discussion to coarse-grained model systems.

3.1 Single chain behavior in the bulk

In the limit of infinite chain length, single polymer molecules constitute a well-defined thermodynamic system able to exhibit phase transitions, the most prominent of these is the coil–globule transition of homopolymers. But also for finite chain length important phase-transition-like structural transformations exist, most importantly the folding transition of proteins, *i.e.*, of specific sequences of heteropolymers of amino acids.

3.1.1 Homopolymer chains. One of the early applications of the MuMC approach to polymer problems is given by the work of Noguchi and Yoshikawa where they studied the collapse transition of stiff homopolymer chains.[50] Stiffness effects on the morphology of collapsed polymer chains and polymer aggregates have been a recurring topic in the application of flat-histogram simulations to polymer problems over the last 20 years. Noguchi and Yoshikawa were interested in the ability of simple models for stiff homopolymers to reproduce and predict the non-trivial structure formation, most notably a collapse into a toroidal structure, occurring for some DNA variants. Using MuMC simulations, their model of tangent

hard-sphere chains with a persistent mechanism of flexibility and square-well attractions between the monomers showed a continuous collapse transition for flexible homopolymer chains, which became a first-order transition beyond a certain stiffness value. For very high stiffness, the model exhibited a collapse into a toroidal structure as found in the DNA case, at intermediate stiffnesses toroidal structures and rod-like ordered globules (akin to the lamella folded states of crystallized homopolymers[51]) coexisted. The change from a continuous transition for flexible polymers to a first-order collapse for sufficiently stiff chains was expected on theoretical grounds[52] and was studied for very long chains by Bastolla and Grassberger using the advanced chain-growth Monte Carlo method PERM (pruned enriched Rosenbluth method)[53] for lattice homopolymer models at that time. The qualitative phase diagram for stiff chains, which Noguchi and Yoshikawa found for a continuum polymer model, could be confirmed in a canonical MC simulation of the bond-fluctuation model[54] for similar chain lengths, whereas a study of longer chains needed an extended ensemble MC scheme[55] which also produced other collapsed morphologies (*e.g.*, tennis rackets) as found in, *e.g.*, AFM experiments on polysaccharides.[56] The extremely challenging parts of the phase diagram from the computational point of view are the dense collapsed and potentially ordered states and transitions between them. The elucidation of the equilibrium properties of these states requires the application of the most advanced flat-histogram MC methods as well as carefully designed update moves like end-bridging,[57] double-bridging[58] and pull-moves[59] or MuMC chain-growth methods.[60] Progress in these fields has led to recurring simulation studies and an improved understanding of these structures over the last 20 years.

The first WLMC simulations of single homopolymers[61] were targeted at the determination of the excess entropy of self-avoiding walks compared to random walks and also exhibit a first application of WLMC methods to ring polymers.[62] Rampf *et al.*, in a series of papers[63–65] using WLMC simulation of the bond-fluctuation model, returned to the problem of the collapse transition of a homopolymer chain. In ref. 63 and 64 they showed that the coil–globule transition can be of first order, and not continuous as believed until then, when the range of the attractive interaction becomes short enough. Parsons *et al.*[66] found no such first-order collapse for a continuum model with Lennard-Jones interactions, but also did not determine the density of states to low enough energies to identify the first-order freezing transition in the collapsed globule, which was identified in ref. 65 for the bond-fluctuation model and a longer range of attractive interactions compared to ref. 63 and 64. A detailed study of the effect of the interaction range was then presented for a continuum model by Taylor *et al.*[67,68] using flexible tangent hard-sphere chains with square-well attractions. These works established that for every fixed chain length, N, there is a range of the attractive interaction, $\lambda_c(N)$, where the collapse transition changes from first order (for $\lambda < \lambda_c(N)$) to second order (for $\lambda > \lambda_c(N)$), a finding supported by simulations using a variant of the MuMC method

applied to a continuum chain model.[69] This behavior carries over to the thermodynamic limit and $\lambda_c(N) \to \lambda_c(\infty)$ at which value the liquid phase gets destabilized for $\lambda < \lambda_c(\infty)$ due to the shortness of the attraction and only the gas phase (coil) and solid phase (ordered globule) survive.

Let us discuss the analysis of flat-histogram simulations from which the above results were obtained. The main result of flat-histogram simulations is the micro-canonical entropy, *i.e.*, the logarithm of the density of states. This function is plotted for several models on the top of Fig. 2 to give an idea about its typical shape. For the tangent square-well spheres chain the range of the attractive interaction is set to $\lambda = 1.1$ (the hard-sphere diameter of the monomers is set to $\sigma = 1$, the bond length also).[67,68] For the fused square-well spheres chain the bond length is set to $l = 0.6$. The third density of states is from a lattice model, the bond-fluctuation model[63,64] and for chain length $N = 256$. All models exhibit a maximum degeneracy for energies below the maximum energy value, a finite size artefact leading to negative micro-canonical temperatures for energies larger than the location of the maximum. The $S(E)$ curves are
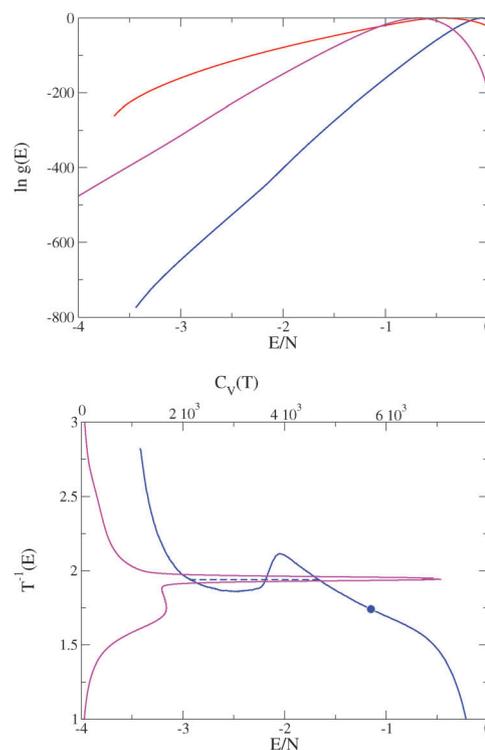
Fig. 2 Top: Micro-canonical entropies (*i.e.*, the logarithm of the density of states) as a function of energy per monomer for a tangent square-well spheres chain of length $N = 128$ (blue curve), a fused square-well spheres chain (bond length $l = 0.6$) of length $N = 40$ (red curve) and a bond-fluctuation model lattice chain of length $N = 256$ (green curve). Bottom: Micro-canonical temperature (blue curve) as a function of energy per monomer for the tangent square-well spheres chain from the top figure. Also shown is the canonical specific heat for this chain (values on top, magenta curve) *vs.* the inverse temperature. The Maxwell-like construction for the inverse temperature curve determines a first-order crystallization transition, the isolated inflection point (filled blue circle) a second-order collapse transition.

rather non-descriptive, but contain all thermodynamic information on the model system. For all of them, there exist convex regions (so-called convex intruders) for certain values of the energy which indicate a first-order phase transition region, in which energy values connected by a common tangent construction to the $S(E)$ curves denote coexisting phases. The phase transitions are most easily analyzed for finite chain length N in the micro-canonical ensemble,[70–73] e.g., by the behavior of the inverse micro-canonical temperature, $T^{-1} = dS(E)/dE$, shown on the bottom of Fig. 2 for the tangent square-well spheres chain. The common tangent construction here leads to a Maxwell-like loop (dashed blue line), whereas a second-order phase transition is indicated by an isolated inflection point (filled blue circle) of the curve. With decreasing interaction range this inflection point moves into the coexistence loop of the first-order transition, meaning that the transition from the random coil to the liquid globule becomes metastable and a direct transition from a random coil to an ordered (in this case fcc ordered) globule occurs.[67]

From the micro-canonical density of states, the canonical partition function is determined by a Laplace transform $Z(T) = \sum_E g(E) \exp(-\beta E)$ and from this partition function all thermodynamic functions in the canonical ensemble can be calculated, e.g., $F(T) = -k_B T \ln[Z(T)]$. In the canonical ensemble the phase transformations of the chains can be most easily identified as peaks in the specific heat, $C(T) = \partial E/\partial T = -T \partial^2 F/\partial T^2$ (magenta curve in the bottom part of Fig. 2). The transition temperatures obtained from the micro-canonical and the canonical analysis do not agree for finite chain length (system size) but do so in the thermodynamic limit $N \to \infty$. From such a combined canonical and micro-canonical analysis of the collapse transition of flexible chains the phase diagram as a function of attraction range arises shown in Fig. 3. In the infinite chain length limit, the tricritical point in this figure moves to $\lambda_c(\infty) = 1.15$.
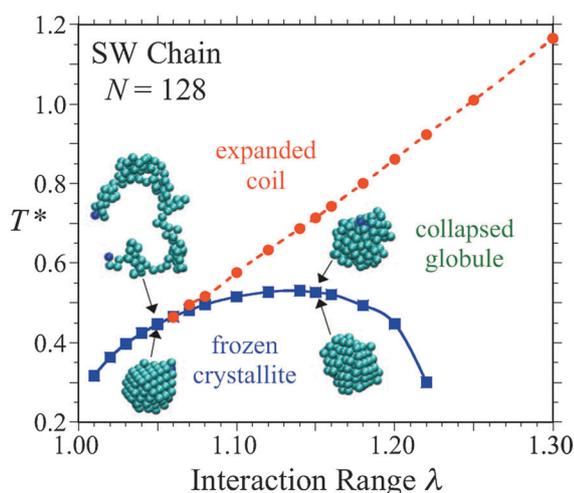
Fig. 3 Phase diagram of a tangent hard-spheres chain with square-well attraction in the temperature–interaction range plane. The diagram is for chain length N = 128, but the topology survives in the thermodynamic limit (taken from ref. 67).

Incidentally, this value is identical to the value where the liquid phase becomes unstable for colloidal systems with a square-well attraction.[74] Due to the correspondence between the single chain phase diagram and the polymer solution phase diagram, the latter will also exhibit a vanishing dense solution phase at this crossover.

An alternative way of analyzing the phase behavior within the canonical ensemble consists in determining the Fisher zeros of the partition function in the complex temperature plane.[75] This approach delivers consistent results to the micro-canonical or standard canonical ones.

The fcc crystal in the ordered state of the collapsed globule occurring for the tangent hard-sphere chains is reminiscent of the crystal structures occurring in Lennard-Jones clusters, and this analogy has been analyzed in detail by Schnabel et al.[25,76] using MuMC simulations and by Seaton et al.[77] using WLMC simulations. For finite chain lengths, the surface to volume ratio of the globular state is not small, and thus reordering transitions occurring at the surface of the globule lead to prominent low-temperature peaks in the specific heat of the system, similar to finite-size rounded first-order peaks.[78] Schnabel et al. found magic chain lengths corresponding to magic numbers in Lennard-Jones clusters, where stable icosahedral ground-state structures are populated. With growing chain length a next shell around the icosahedral structure is started in an anti-Mackay fashion (hcp-like ordering) giving way to a closure of this shell before the next magic chain length in a Mackay fashion (fcc-like ordering), where we used nomenclature of the classification of Lennard-Jones clusters. In the thermodynamic limit these transitions no longer contribute (as pure surface effects) and one is left with bulk crystallization into an fcc ground state as also found in ref. 67.

When the macromolecule is enclosed in a cavity of linear extent comparable to its (free) radius of gyration the characteristics of the coil–globule transition may be modified by confinement effects. The transition to the ordered state of the collapsed globule, on the other hand, is usually hardly affected by the confinement because in both the ordered and disordered globular state the polymer is compact and hence usually smaller than the confinement scale. A prominent example is the folding behavior of proteins in a cellular environment, for which an increase of the folding temperature due to the confinement has been reported.[79] A similar effect was observed in a MuMC simulation for the coil–globule transition of a simple flexible polymer in a spherical cavity,[80] albeit just in the opposite temperature direction. One plausible reason for this difference is that proteins are much stiffer than the polymer simulated in ref. 80. This explanation has recently been supported by further MuMC simulations including an explicit bending stiffness term.[81]

Let us hence return now to the question of stiffness effects on the structure of collapsed polymers with which we started this section. One point to note is that not all stiffnesses are created equal. Using a rotational isomeric state like stiffness with anisotropic interactions based on torsional degrees of freedom, Kemp et al.[82] with MuMC simulations and Varshney et al.[83]

with WLMC simulations studied the helix–coil transition of stiff polymers. Later Magee *et al.*[84] showed that this transition can even be introduced by isotropic interactions, when one introduces stiffness by studying fused-sphere models, *i.e.*, models where the size of the monomer is larger than the bond length, a finding later also reported from WLMC simulations.[15] However, here the helical state is only stable for very short chains, changing into stems wrapped by helices for longer chains. Employing instead angle potentials with 180 degrees as the minimal energy structure (persistent mechanism of flexibility), Siretskiy *et al.*[85] and Seaton *et al.*[86] using a WLMC simulations to generate a two-dimensional density of states depending on stiffness energy and attraction energy, reproduced the collapsed morphologies found in ref. 54 for the same class of stiffness potentials. In recent MuMC simulations combined with parallel tempering (in an ''orthogonal'' parameter direction) thermodynamically stable phases exhibiting knotted conformations of various knot types have been identified.[87] However, the results obtained so far are diagrams of states for fixed finite chain length only, and the chain length dependence of these diagrams and the extrapolation to the thermodynamic limit have not been studied yet. Clearly, the asymptotically stable structures will be determined by the competition between bending energy and non-bonded energy with respect to the thermal energy, but which ordered structures are favored in which region of this two-dimensional phase space in the thermodynamic limit is still an open question.

Besides these studies of linear homopolymers, flat-histogram simulations have also been used to study the phase behavior of rings,[62] star polymers[88] and dendrimers.[89] For the rings, only relatively short chains ($N \leq 50$) have been studied so far and the main qualitative finding is that the strength of the coil–globule transition relative to low-temperature ordering transitions is reduced compared to linear chains of the same length. The study of star polymers was performed using the bond fluctuation model with an interaction range equal to the one used in ref. 63 and 64. Wang *et al.*[88] confirmed the results for linear chains and showed that the scaling curve $T_{\mathrm{cryst}}(N) - T_{\mathrm{cryst}}(\infty) \simeq N^{-1/3}$ for the finite-size shift of the liquid-to-crystal transition is independent on the functionality of the stars between 2 (linear chains) and 12 arms. They also found that the choice of interaction range $d = \sqrt{6}$ for this model yields the tricritical point where the coil–globule and liquid–crystal transitions occur at the same temperature. This finding is also compatible with the results by Wang *et al.*[89] for dendrimers, although the limited size range and stronger fluctuations did not allow a quantitative analysis of the thermodynamic limit there.

Another very active research field are studies of polymers in disordered environments where one investigates the polymer statistics in the presence of obstacles or impurities. It is often a reasonable approximation to consider the dynamics of the obstacles to be static (or at least much slower than the polymer fluctuations), which allows one to apply the so-called quenched approximation. The randomly placed obstacles then act as a kind of ''excluded volume'' constraint for the polymer statistics which leads to a very rugged free-energy landscape with many rare-event states (*e.g.*, squeezing the polymer through very small channels between two obstacles is very unlikely). By artificially softening these hard ''excluded volume'' potentials in a special variant of MuMC, this landscape can be successfully flattened. This was first demonstrated for flexible[90] and semi-flexible[91] polymers moving in uncorrelated disorder by comparison with an especially designed chain-growth algorithm.[92] More recently this method has been applied to study semi-flexible polymers of worm-like chain type in the (correlated) disordered background of a quenched hard-disk fluid.[93] As the main result of this study it was found that the semi-flexible polymer still exhibits effective worm-like chain statistics, but with a renormalized (smaller) persistence length. A simple empirical relation between this renormalized persistence length and the original ''thermal'' persistence length defines a novel quantitative measure of molecular crowding which suggests that it may be possible to use semi-flexible polymers as a local probe of material microstructure.[93]

3.1.2 Heteropolymers and simplified protein models. There are two main classes of heteropolymers studied in the literature. In HP models, where H = hydrophobic and P = polar repeat units make up the chain, the H units have an attractive interaction among themselves, whereas the P units only have excluded volume interactions with all other groups. In AB models there are attractive AA and BB interactions (usually taken as equal) and only repulsive interactions between A and B units. The HP model is generally studied on the lattice and the AB model more in the continuum, but both can be defined in discrete and continuous versions. The HP model is built to capture the hydrophobic demixing from a polar solvent, while the AB model captures demixing between A and B in neutral solvent.

When one distributes few attractive H monomers (regularly) along a P chain, one has a chain with sticker monomers. This was studied with MuMC simulations in two dimensions for a lattice model in ref. 94 and in three dimensions for continuum models in ref. 95 and 96. In ref. 96 a regular chain of type $(\mathrm{HPPP})_n$ was studied and shown to exhibit micelle formation of the H units. For a long enough chain the collapse proceeds through two (for the longest chains simulated in this work) stages: a formation of two micellar cores in the first stage of the collapse which then aggregate at lower temperatures in a second stage. The difference between the HP and AB heteropolymers concerning their collapsed morphologies was emphasized in a work studying regular $(\mathrm{X}_m\mathrm{Y}_m)_n$ heteropolymers.[97] For the AB model the structures have to be symmetric under the exchange of A and B, whereas for the HP model they are not. Both models also show different trends in the nature of the transitions as a function of the block length m. For $m = 1$, an alternating copolymer, the collapse transition is continuous in the HP model and strongly first order in the AB model. It then gets first order in the HP model beyond block length $m = 4$, with a decreasing width of the transition as function of the energy per monomer. In the AB model, on the contrary, the first-order character weakens with increasing m until a two-stage collapse occurs around $m = 8$, and both transitions seem to merge for still larger m.[97]

The HP model is best known as a strongly simplified protein model, obtained when the sequence of amino acids making up a protein or short peptide is translated into a binary alphabet only depending on whether an amino acid is classified as hydrophilic or hydrophobic. In this case one has random-looking (but not binomial[98]) sequences of H and P units with a fixed length determined by the given protein one tries to model. For these simulations the question of a possible thermo-dynamic limit can not be posed and one has to study the properties of each finite, individual sequence. One of the most important properties of these sequences is their ground-state energy, and it could be shown that both, MuMC simula-tions[99,100] using a MuMC PERM implementation[60] and WLMC simulations[101,102] using an advanced move set[57–59] were able to reproduce or even improve the ground-state estimates for designed HP sequences in the literature up to chain lengths of $N = 136$. These general simulation approaches were therefore in this aspect competitive with the best specialized ground-state searches applied to these chains. The same behavior was found for HP models on 2d and 3d fcc lattices.[103] However, the main result of the flat-histogram simulations, as always, was the density of states and with that the complete thermal diagram of states of these model chains. For these lattice simulations, the diagram of states always showed two transi-tions, the hydrophobic collapse (coil–globule transition in the homopolymer case) followed by a transition to the native state (liquid-to-crystal transition in the homopolymer case) at a lower temperature. In a recent large-scale WLMC simulation also the probability of knotting under native (ground-state-like) condi-tions for random HP sequences with 500 residues has been investigated.[104] On average the lattice peptides are found almost as knotted as globular homopolymers of comparable density, but the introduction of sequence leads to a large variability in the self-entanglements of heteropolymers.

These lattice based HP models do not show the two-state folding often found for short proteins and peptides, whose thermodynamics could be reproduced in a simple homo-polymer chain model for short enough interaction range.[68] From this observation one can draw a speculative explanation for this failing of the HP models: the interaction range in these (typically simple cubic) lattice models is equal to the exclusion size of the monomers, i.e., much larger than the range needed for a first-order coil–crystal (native state) transition, which is about 10% of the hard-core extension of the monomers. To introduce two-state folding behavior for such chains, Gō-like model features with energy penalties for deviations from the native structure have to be introduced,[105] or one can introduce a first-order transition by inclusion of chain stiffness, as was done in ref. 24 for an AB model in the continuum. This is illustrated in Fig. 4, which shows the results for three simple AB sequences with 20 monomers exhibit-ing (a) two-state folding, (b) folding through intermediates, as well as (c) glass-like metastability. Finally, mimicking the experimental approach to explore the properties (especially the aggregation tendency) of proteins by point mutations of selected amino acids in the sequence, the stability of the phase behavior of HP chains under such mutations has also been studied.[106]
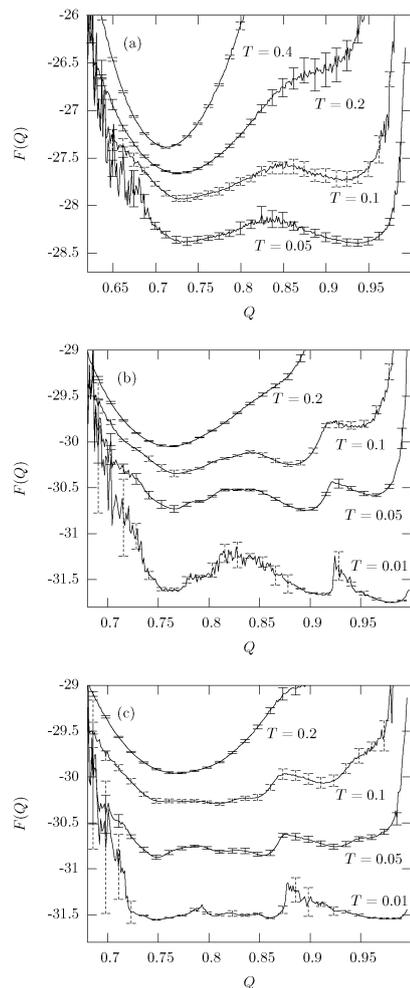
Fig. 4   Free energy (up to an unimportant constant) as a function of the overlap parameter Q for three AB sequences exhibiting (a) two-state folding, (b) folding through intermediates, and (c) glass-like metastability (taken from ref. 24).

3.2   Single chains at surfaces

For many applications like surface coatings or colloidal stabili-zation, the behavior of polymers at interfaces is of high rele-vance, as is also true for the interaction of proteins with surfaces. From the basic science point of view, single chains at surfaces introduce an interesting competition between three-dimensional phase transitions, two-dimensional phase transitions and the adsorption transition of the chains onto the surface. For this reason, in the last ten years many flat-histogram MC simulations have been devoted to this problem. Two lines of approach have been followed in these investigations: in the first one a chain next to an attractive wall and confined by a second repulsive wall at sufficiently large distance to the first wall has been studied, i.e., a slit geometry; in the second line, tethered chains (one end grafted to an attractive wall) in an infinite half-space have been analyzed, the classical model for studying the adsorption transi-tion in polymer physics. Both approaches differ in the contribu-tion of the translational entropy of the chain, which depends on the distance between the walls in the slit geometry.

For homopolymer chains, the slit geometry has been studied for a two-dimensional system in ref. 107 and for a three-dimensional system in ref. 108–111 whereas the tethered geometry has been studied in ref. 112–115. In both geometries the three phases in 3d, coil, liquid globule and ordered globule (for large enough interaction range) exist also in this case, but in addition for very strong attraction to the surface, the quasi two-dimensional chains show the corresponding 2d phases (however, the nature of the 2d crystallization transition of single polymer chains has not been analyzed yet). The two regimes are separated as a function of attraction strength to the surface by the adsorption transition. Close to this critical value of the surface attraction, the chains are adsorbed but not completely two-dimensional leading to further layering transitions, especially of adsorbed ordered structures. A typical diagram of states for a polymer chain at an attractive wall is shown in Fig. 5. Adsorbed phases are indicated by the letter "A", desorbed by "D", extended states by "E", globular states by "G" and compact ordered states by "C". For a related study comparing canonical and micro-canonical analysis of non-grafted homopolymer adsorption, see ref. 116 and 117.

The main difference between the two confining geometries occurs for the adsorption transition. Möddel et al.[109] in a study of a semi-flexible continuum chain found that the adsorption transition in the slit geometry can be of first order for short chains, turning second order in the thermodynamic limit. This is in contrast to the tethered case, where this transition is always continuous. The difference is caused by the importance of the translational entropy in the slit case. Furthermore Möddel et al. argued that the adsorption temperature in the slit geometry should be inversely proportional to $N^{-1}\ln L_z$, where N is the chain length and L_z the distance between the walls. For every fixed N the transition temperature in the slit geometry in the dilute limit $L_z \to \infty$ therefore goes to zero. The nature of this phase diagram also did not depend on whether a short-ranged[108,112] or long-ranged van der Waals like[109,114] attraction to the surface was used. A simulation at finite, adjustable concentration (i.e., distance L_z between the slits) of

a simplified model for a polyelectrolyte in solution with its counter ions was performed by Volkov et al.[111] where they determined a two-dimensional density of states $g(E,V)$ depending on energy and volume. The main adsorption properties are also preserved when one considers a polymer confined inside a spherical cavity attracted by the inner wall of the sphere.[118] Here the usually employed 9-3 Lennard-Jones surface potential for a flat substrate (resulting from integrating a 12-6 Lennard-Jones potential over the lower half space) has to be replaced by a 10-4 Lennard-Jones surface potential (due to integrating over the spherical surface). By an appropriate matching of the coupling constants it can be theoretically argued that this difference does not matter much[119] and MuMC simulations do confirm this expectation.[118]

Of high practical importance is the adsorption of polymers on patterned surfaces, for instance for sensor applications. Möddel et al.[120] studied this for the adsorption of a homopolymer of length $N = 40$ onto a surface with a stripe pattern. The adsorption phase diagram of a homopolymer next to a homogeneously attractive surface is modified, because now the adsorption to the surface out of the different three-dimensional equilibrium structures (coil, globule, frozen) takes place with a concomitant recognition of the surface pattern by the polymer. For dominating attraction to the stripe, the polymer is extended into a rod-like structure in the adsorption process. Such structures were also found in a variation to a hard-wall confinement, where the phase behavior of a polymer chain next to a (flat) membrane was studied.[121] For very stiff membranes, the findings reproduced the behavior at a hard wall, as expected. For flexible membranes, a new adsorbed state occurred, where the membrane tries to wrap around the adsorbed polymer. When the intramolecular interaction of the polymer wins, the membrane wraps around a compact, collapsed chain. For strong attraction to the membrane (which was a square-lattice net), the chain adsorbed in an extended configuration maximizing the monomer–membrane contacts. Such behavior may depend on the local commensurability of the membrane and the polymer, however.

3.3 Chain aggregates

Folding of proteins or the collapse of polymers are among the most prominent phase transformations of single macromolecules. In general, for an ensemble of a few interacting proteins or polymers also the interplay with aggregation plays an important role. In fact, for biopolymers, aggregation is one of the most relevant molecular structure formation processes. An important and extensively studied example is the extracellular aggregation of the Aβ peptide, which is associated with Alzheimer's disease. Aiming at an understanding of the basic mechanism of this process, Junghans et al.[72,122] considered a coarse-grained bead-stick HP model in the continuum (also often referred to as "AB model"), where each residue is represented by only a single interaction site, the "Cα atom". In particular they considered a short 13-mer with sequence AB$_2$AB$_2$ABAB$_2$AB (representing a Fibonacci sequence) whose single-chain properties were already well studied.[100] The intermolecular interactions among the various peptides were

Fig. 5 Qualitative phase diagram of homopolymer chains next to an attractive surface moving either freely in a three-dimensional slit geometry ("free") or in a tethered geometry where one end of the polymer is fixed on the surface ("grafted") (taken from ref. 115).

assumed to be of the same 12-6 Lennard-Jones type as the intramolecular interactions among the monomers or residues of a single peptide. By confining M peptide chains in a cubic box of edge length L (= 40) with periodic boundary conditions, the relevant phase space could be completely covered by MuMC simulations. As outlined above this allows one to analyze the system from both the canonical and micro-canonical perspective. In order to distinguish between the fragmented and aggregated regime, an order parameter $\Gamma^2 = \sum_{i,j} \left(\vec{r}_{\rm cm}^i - \vec{r}_{\rm cm}^j \right)^2 \big/ 2M^2$ (with implicit minimal-distance convention for periodic boundary conditions) was introduced that adopts the definition of the squared radius of gyration for a single polymer and basically measures the average spread of the center-of-mass distances $|\vec{r}_{\rm cm}^i - \vec{r}_{\rm cm}^j|$ of the M chains. In the aggregated phase, one thus expects $\Gamma^2 \approx 0$, whereas in the fragmented phase Γ^2 approaches a non-zero value.

Measuring the energy and specific heat as well as Γ^2 and its temperature derivative for systems with 2, 3, and 4 peptides, clear evidence for a first-order-like aggregation transition was obtained. For all three systems considered, the general behavior turned out to be similar. There is only this single transition which indicates that conformational changes of the individual peptides accompany the aggregation process and are not separate transitions, i.e., the hydrophobic core formation and the aggregation transition happen at the same temperature. A closer look for the 4-peptides system revealed, however, that the micro-canonical entropy and temperature derived from the multi-canonical data are so sensitive that a hierarchy of sub-phases in the nucleation transition region can be resolved.[123] Physically these sub-phases can be interpreted as signal that the next peptide starts to join the aggregate. Using similar techniques also the intra-association of hydrophobic segments in a 62 segment heteropolymer chain has been investigated.[124] In ref. 125 the micro-canonical thermostatistics of two isoforms of the amyloid β-protein (the Src SH3 domain and the human prion protein hPrP) was studied by using a coarse-grained model. Emphasis was laid in this work on free-energy barriers and the latent heat in these models, characterizing the amyloidogenic propensity, that is how aggregation-prone the heteropolymers are.

In another MuMC simulation for 4 homopolymer chains of length N = 13 (using the same model as above and formally the sequence A_{13}) it was observed that also in this case the collapse of flexible polymers into the globular state and the aggregation transition happen at the same temperature.[126] In fact, to a good approximation, the aggregated state of M polymers of length N may be viewed as the collapsed globular state of a single polymer of length MN, which explains this coincidence. Along similar lines the aggregation properties of two coarse-grained bead-stick polymers of length N = 22 have been studied in ref. 127. More recently this finding has been confirmed in a more elaborate parallel MuMC study of up to 24 flexible bead-spring polymers of length N = 13, 20, and 27 confined in a spherical cavity.[128] Here the elasticity of the covalent bonds is governed by the finitely extensible nonlinear elastic (FENE)

potential $V_{\rm FENE}(r) = -\dfrac{K}{2}R^2 \ln\left(1 - \left[(r - r_0)/R\right]^2\right)$ with r_0 = 0.7, R = 0.3, and K = 40. In this study particular emphasis was laid on the analogy of the aggregation process to particle condensation[31,129,130] and the finite-size scaling properties of the aggregation transition.

Building on this earlier work mainly for flexible polymers,[72,122,126,128] recently a systematic investigation of the influence of bending stiffness on the polymer aggregation process has been conducted in ref. 131. In this study the same coarse-grained bead-spring model with FENE bonds was employed as in ref. 128, and again it was assumed that the intra- and intermolecular interactions are identical and of 12-6 Lennard-Jones type. As for flexible polymers, the aggregated and separated phases of M semi-flexible polymers can be monitored by the "phase" separation order parameter Γ^2. To distinguish in the semi-flexible case amorphous from bundle-like structures in the aggregated phase an end-to-end correlation order parameter $C_{\rm R} = \dfrac{2}{M(M-1)} \sum_{i<j} \left(\hat{\vec{R}}_i \cdot \hat{\vec{R}}_j \right)^2$ was introduced, where $\hat{\vec{R}}_i$ denotes the end-to-end vector (normalized to unity) of the ith polymer. By performing extensive MuMC simulations in a parallel implementation[27] it could be shown that the bending stiffness plays a crucial role in whether the system forms an amorphous aggregate or a bundle structure.

Fig. 6 shows the resulting temperature–stiffness phase diagram for eight 13-mers exhibiting a regime of rather flexible polymers forming amorphous aggregates, an intermediate regime, and a regime of rather stiff polymers forming bundle-like structures. In
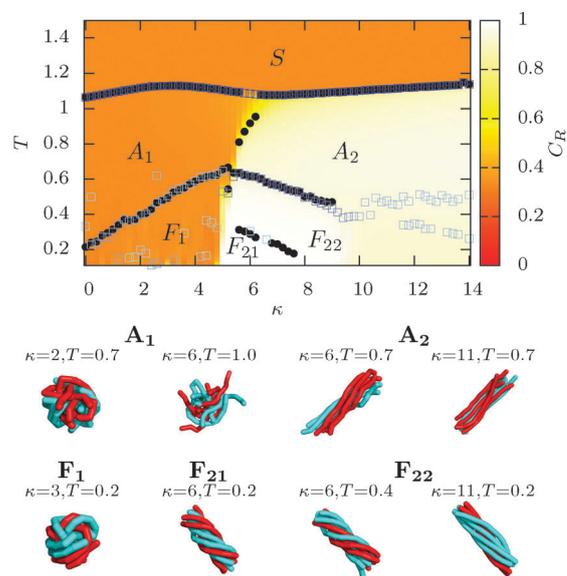
Fig. 6 Aggregation phase diagram for eight 13-mers. Shown are a surface plot of the end-to-end correlation parameter C_R (see text), the maxima of the heat capacity (black dots) and the temperature derivative of the phase separation parameter Γ^2 (blue squares). Several structural phases can be distinguished: S (separated), A (aggregated), and F (frozen). In the lower panel of the figure representative conformations in the low-temperature phases are depicted (taken from ref. 131).

the intermediate stiffness regime a micro-canonical analysis showed that lowering the temperature first drives the system into an uncorrelated aggregate, shortly followed by a second-order-like transition into the correlated aggregate. The "frozen" (low-temperature) states in Fig. 6 show a twisted bundle structure if the stiffness is large enough. This sort of structure has been reported before in the context of material design for specific interactions usually related to proteins. Since the study of ref. 131 did not include any specific interactions, but instead a simple coarse-grained homopolymer model with short-range attraction, hard-core repulsion and additional bending stiffness, it is tempting to conclude that specific interactions are not necessary for bundle formation. Specific interactions such as, *e.g.*, hydrogen bonding may, however, stabilize (or destabilize) the occurring bundle structures.

A class of chain aggregates of increasing importance today are microgels, formed either by chemical or by physical cross linking. In this application so far only more classical simulations have been applied which obtain the density of states of a system by means of histogram reweighting techniques[20,21] over a parameter range usually more limited than possible in MuMC and WLMC simulations. Kumar and Panagiotopoulos[132] used grand-canonical MC simulations of solutions of reversibly associating polymers at different values of temperature and chemical potential to obtain an estimate of the microcanonical partition function of this system through histogram reweighting of these simulations. They found that the gelation transition is a continuous structural transition without thermodynamic signatures. Clearly, further studies of the gelation transition by means of MuMC and WLMC simulations would be possible now and a timely endeavour.

4 Conclusions

Applications of flat-histogram Monte Carlo methods to polymer simulations, be it in the form of the multi-canonical (MuMC), the Wang–Landau (WLMC), or the more recent Stochastic Approximation Monte Carlo (SAMC) scheme, have proven to be an extremely powerful tool for obtaining accurate information on the thermodynamics and structure of single polymer chains and polymer aggregates over broad parameter ranges. Typically these methods are able to give estimates of the density of states which, in turn, may be used as a starting point for micro-canonical considerations that can yield useful complementary information to the more standard canonical data analyses.

From experience with the examples of polymer physics reviewed here and also from the numerous applications to more traditional spin systems in statistical mechanics one obtains the impression that the performance of the two methods, MuMC and WLMC, is qualitatively comparable. A more quantitative comparison is rather difficult since both methods depend on quite a few parameters that govern their performance in a subtle way and render a detailed and fair comparison quite cumbersome. The pros and cons of the two methods are also very sensitive to the specific model under study and the considered ranges of the physics parameters.

The great success of flat-histogram methods was only possible, however, through a judicious choice of update proposal moves, which for polymers can be quite a tricky issue. In fact, in many applications this ingredient of flat-histogram Monte Carlo simulations can be most important to achieve convergence of the method. Even with the most advanced algorithmic and move choices, however, the methods fight against one problem which is underlying the foundations of statistical physics: the entropy is an extensive thermodynamic variable and thus the density of states grows exponentially in the number of particles one is considering. For long single chains in a continuum model this already led to variations of the density of states over 3000 orders of magnitude,[25,26] whereas a recent study of a melt of short semi-flexible chains[133] with 7200 monomers needed to determine a density of states over 5000 orders of magnitude. And the models used in these works were simplified, coarse-grained polymer models. Obviously, this poses great challenges when attempting to extend such approaches to chemically realistic polymer models and more complicated situations which will require further algorithmic advances to become feasible. Among others, these include a judicious choice of energy ranges, energy dependent update moves (with bias corrections), optimized convergence procedures, and also more refined parallelization schemes to fit flat-histogram Monte Carlo methods perfectly into the architecture of modern high-capability computers.

Acknowledgements

References

1 M. P. Allen and D. J. Tildesley, *Computer Simulation of Liquids*, Oxford University Press, Oxford, 1987.

2 D. Frenkel and B. Smit, *Understanding Molecular Simulation: From Algorithms to Applications*, Academic Press, New York, 2nd edn, 2001.

3 D. C. Rapaport, *The Art of Molecular Dynamics Simulations*, Cambridge University Press, Cambridge, 2nd edn, 2004.

4 M. E. J. Newman and G. T. Barkema, *Monte Carlo Methods in Statistical Physics*, Clarendon Press, Oxford, 1999.

5 D. P. Landau and K. Binder, *Monte Carlo Simulations in Statistical Physics*, Cambridge University Press, Cambridge, 2000.

6 B. A. Berg, *Markov Chain Monte Carlo Simulations and Their Statistical Analysis*, World Scientific, Singapore, 2004.

7 W. Janke, Monte Carlo simulations in statistical physics – from basic principles to advanced applications, in *Order,*

Disorder and Criticality: Advanced Problems of Phase Transition Theory, ed. Y. Holovatch, World Scientific, Singapore, 2012, vol. 3, pp. 93–166.

8 G. M. Torrie and J. P. Valleau, *J. Comput. Phys.*, 1977, **23**, 187–199.

9 B. A. Berg, *Fields Inst. Comm.*, 2000, **26**, 1–24; B. A. Berg, *Comput. Phys. Commun.*, 2002, **147**, 52–57.

10 W. Janke, *Physica A*, 1998, **254**, 164–178; W. Janke, *Lect. Notes Phys.*, 2008, **739**, 79–140.

11 U. H. E. Hansmann and Y. Okamoto, in *Annual Reviews of Computational Physics VI*, ed. D. Stauffer, World Scientific, Singapore, 1999, pp. 129–157.

12 P. N. Vorontsov-Velyaminov, N. A. Volkov, A. A. Yurchenko and A. P. Lyubartsev, *Polym. Sci., Ser. A*, 2010, **52**, 742–760.

13 T. Wüst, Y. W. Li and D. P. Landau, *J. Stat. Phys.*, 2011, **144**, 638–651.

14 S. Singh, M. Chopra and J. J. de Pablo, *Annu. Rev. Chem. Biomol. Eng.*, 2012, **3**, 369–394.

15 M. P. Taylor, W. Paul and K. Binder, *Polym. Sci., Ser. C*, 2013, **55**, 23–38.

16 B. A. Berg and T. Neuhaus, *Phys. Lett. B*, 1991, **267**, 249–253.

17 B. A. Berg and T. Neuhaus, *Phys. Rev. Lett.*, 1992, **68**, 9–12.

18 K. Binder, in *Phase Transitions and Critical Phenomena*, ed. C. Domb and M. S. Green, Academic Press, London, 1976, vol. 5b, pp. 1–105.

19 W. Janke, *Int. J. Mod. Phys. C*, 1992, **3**, 1137–1146.

20 A. M. Ferrenberg and R. H. Swendsen, *Phys. Rev. Lett.*, 1988, **61**, 2635–2638; A. M. Ferrenberg and R. H. Swendsen, *Phys. Rev. Lett.*, 1989, **63**, 1658(E); A. M. Ferrenberg and R. H. Swendsen, *Phys. Rev. Lett.*, 1989, **63**, 1195–1198.

21 S. Kumar, J. M. Rosenberg, D. Bouzida, R. H. Swendsen and P. A. Kollman, *J. Comput. Chem.*, 1992, **13**, 1011–1021.

22 D. Chandler, *Introduction to Modern Statistical Mechanics*, Oxford University Press, Oxford, 1987, pp. 168–175.

23 U. H. E. Hansmann and Y. Okamoto, *J. Comput. Chem.*, 1993, **14**, 1333–1338.

24 S. Schnabel, M. Bachmann and W. Janke, *J. Chem. Phys.*, 2007, **126**, 105102.

25 S. Schnabel, M. Bachmann and W. Janke, *J. Chem. Phys.*, 2009, **131**, 124904.

26 S. Schnabel, W. Janke and M. Bachmann, *J. Comput. Phys.*, 2011, **230**, 4454–4465.

27 J. Zierenberg, M. Marenz and W. Janke, *Comput. Phys. Commun.*, 2013, **184**, 1155–1160.

28 V. V. Slavin, *Low Temp. Phys.*, 2010, **36**, 243–249.

29 A. Ghazisaeidi, F. Vacondio and L. A. Rusch, *J. Lightwave Technol.*, 2010, **28**, 79–90.

30 J. Zierenberg, M. Marenz and W. Janke, *Phys. Procedia*, 2014, **53**, 55–59.

31 J. Zierenberg, M. Wiedenmann and W. Janke, *J. Phys.: Conf. Ser.*, 2014, **510**, 012017.

32 B. A. Berg, U. Hansmann and T. Neuhaus, *Phys. Rev. B: Condens. Matter Mater. Phys.*, 1993, **47**, 497–500.

33 B. A. Berg, U. Hansmann and T. Neuhaus, *Z. Phys. B: Condens. Matter*, 1993, **90**, 229–239.

34 B. A. Berg and W. Janke, *Phys. Rev. Lett.*, 1998, **80**, 4771–4774.

35 B. A. Berg, A. Billoire and W. Janke, *Phys. Rev. B: Condens. Matter Mater. Phys.*, 2000, **61**, 12143–12150.

36 F. Wang and D. P. Landau, *Phys. Rev. Lett.*, 2001, **86**, 2050–2053.

37 F. Wang and D. P. Landau, *Phys. Rev. E: Stat., Nonlinear, Soft Matter Phys.*, 2001, **64**, 056101.

38 Q. Yan, R. Faller and J. J. de Pablo, *J. Chem. Phys.*, 2002, **116**, 8745–8749.

39 C. Zhou and R. N. Bhatt, *Phys. Rev. E: Stat., Nonlinear, Soft Matter Phys.*, 2005, **72**, 025701(R).

40 Q. Yan and J. J. de Pablo, *Phys. Rev. Lett.*, 2003, **90**, 035701.

41 D. P. Landau, S.-H. Tsai and M. Exler, *Am. J. Phys.*, 2004, **72**, 1294–1302.

42 R. A. Belardinelli and V. D. Pereyra, *Phys. Rev. E: Stat., Nonlinear, Soft Matter Phys.*, 2007, **75**, 046701.

43 R. A. Belardinelli and V. D. Pereyra, *J. Chem. Phys.*, 2007, **127**, 184105.

44 A. D. Swetnam and M. P. Allen, *J. Comput. Chem.*, 2010, **32**, 816–821.

45 F. Liang, *J. Stat. Phys.*, 2006, **122**, 511–529.

46 F. Liang, C. Liu and R. J. Carroll, *J. Am. Stat. Assoc.*, 2007, **102**, 305–320.

47 F. Liang, *Statist. Prob. Lett.*, 2009, **79**, 581–587.

48 B. Werlich, T. Shakirov and W. Paul, *Comput. Phys. Commun.*, 2015, **86**, 65–70.

49 T. Vogel, Y. W. Li, T. Wüst and D. P. Landau, *Phys. Rev. Lett.*, 2013, **110**, 210603; T. Vogel, Y. W. Li, T. Wüst and D. P. Landau, *Phys. Rev. E: Stat., Nonlinear, Soft Matter Phys.*, 2014, **90**, 023302.

50 H. Noguchi and K. Yoshikawa, *Chem. Phys. Lett.*, 1997, **278**, 184–188; H. Noguchi and K. Yoshikawa, *J. Chem. Phys.*, 1998, **109**, 5070–5077.

51 G. Strobl, *The Physics of Polymers*, Springer, Berlin, 2007.

52 A. Yu. Grosberg and A. R. Khokhlov, *Statistical Physics of Macromolecules*, American Institute of Physics, New York, 1994.

53 U. Bastolla and P. Grassberger, *J. Stat. Phys.*, 1997, **89**, 1061–1078.

54 V. A. Ivanov, W. Paul and K. Binder, *J. Chem. Phys.*, 1998, **109**, 5659–5669; M. R. Stukan, V. A. Ivanov, A. Yu. Grosberg, W. Paul and K. Binder, *J. Chem. Phys.*, 2003, **118**, 3392–3400.

55 J. A. Martemyanova, M. R. Stukan, V. A. Ivanov, M. Müller, W. Paul and K. Binder, *J. Chem. Phys.*, 2005, **122**, 174907.

56 G. Maurstad and B. T. Stokke, *Biopolymers*, 2004, **74**, 199–213.

57 P. V. Pant and D. N. Theodorou, *Macromolecules*, 1995, **28**, 7224–7234.

58 N. C. Karayiannis, V. G. Mavrantzas and D. N. Theodorou, *Phys. Rev. Lett.*, 2002, **88**, 105503.

59 N. Lesh, M. Mitzenmacher and S. Whitesides, *A complete and effective move set for simplified protein folding, in RECOMB'03*, ACM, New York, 2003, pp. 188–195.

60 M. Bachmann and W. Janke, *Phys. Rev. Lett.*, 2003, **91**, 208105.

61 P. N. Vorontsov-Velyaminov, N. A. Volkov and A. A. Yurchenko, *J. Phys. A: Math. Gen.*, 2004, **37**, 1573–1588.

62 N. A. Volkov, A. A. Yurchenko, A. P. Lyubartsev and P. N. Vorontsov-Velyaminov, *Macromol. Theory Simul.*, 2005, **14**, 491–504.

63 F. Rampf, W. Paul and K. Binder, *Europhys. Lett.*, 2005, **70**, 628–634.

64 F. Rampf, K. Binder and W. Paul, *J. Polym. Sci., Part B: Polym. Phys.*, 2006, **44**, 2542–2555.

65 W. Paul, T. Strauch, F. Rampf and K. Binder, *Phys. Rev. E: Stat., Nonlinear, Soft Matter Phys.*, 2007, **75**, 060801R.

66 D. F. Parsons and D. R. M. Williams, *J. Chem. Phys.*, 2006, **124**, 221103.

67 M. P. Taylor, W. Paul and K. Binder, *J. Chem. Phys.*, 2009, **131**, 114907.

68 M. P. Taylor, W. Paul and K. Binder, *Phys. Rev. E: Stat., Nonlinear, Soft Matter Phys.*, 2009, **79**, 050801(R).

69 J. Gross, T. Neuhaus, T. Vogel and M. Bachmann, *J. Chem. Phys.*, 2013, **138**, 074905.

70 D. H. E. Gross, *Microcanonical Thermodynamics*, World Scientific, Singapore, 2001.

71 W. Janke, *Nucl. Phys. B, Proc. Suppl.*, 1998, **63A–C**, 631–633.

72 C. Junghans, M. Bachmann and W. Janke, *Phys. Rev. Lett.*, 2006, **97**, 218103.

73 W. Paul, F. Rampf, T. Strauch and K. Binder, *Comput. Phys. Commun.*, 2008, **178**, 17–20.

74 M. G. Noro and D. Frenkel, *J. Chem. Phys.*, 2000, **113**, 2941–2944.

75 M. P. Taylor, P. P. Aung and W. Paul, *Phys. Rev. E: Stat., Nonlinear, Soft Matter Phys.*, 2013, **88**, 012604.

76 S. Schnabel, T. Vogel, M. Bachmann and W. Janke, *Chem. Phys. Lett.*, 2009, **476**, 201–204.

77 D. T. Seaton, T. Wüst and D. P. Landau, *Comput. Phys. Commun.*, 2009, **180**, 587; D. T. Seaton, T. Wüst and D. P. Landau, *Phys. Rev. E: Stat., Nonlinear, Soft Matter Phys.*, 2010, **81**, 011802.

78 T. Vogel, M. Bachmann and W. Janke, *Phys. Rev. E: Stat., Nonlinear, Soft Matter Phys.*, 2007, **76**, 061803.

79 D. K. Klimov, D. Newfield and D. Thirumalai, *Proc. Natl. Acad. Sci. U. S. A.*, 2002, **99**, 8019–8024; M. Friedel, D. J. Sheeler and J.-E. Shea, *J. Chem. Phys.*, 2003, **118**, 8106–8113; F. Takagi, N. Koga and S. Takada, *Proc. Natl. Acad. Sci. U. S. A.*, 2003, **100**, 11367–11372; N. Rathore, T. A. Knotts IV and J. J. de Pablo, *Biophys. J.*, 2006, **90**, 1767–1773.

80 M. Marenz, J. Zierenberg, H. Arkın and W. Janke, *Condens. Matter Phys.*, 2012, **15**, 43008.

81 M. Marenz and W. Janke, *Phys. Procedia*, 2014, **57**, 53–57.

82 J. P. Kemp and Z. Y. Chen, *Phys. Rev. Lett.*, 1998, **81**, 3880–3883.

83 V. Varshney, T. E. Dirama, T. Z. Sen and G. A. Carri, *Macromolecules*, 2004, **37**, 8794–8804.

84 J. E. Magee, V. R. Vasquez and L. Lue, *Phys. Rev. Lett.*, 2006, **96**, 207802.

85 A. Siretskiy, C. Elvingson, P. Vorontsev-Velyaminov and M. O. Khan, *Phys. Rev. E: Stat., Nonlinear, Soft Matter Phys.*, 2011, **84**, 016702.

86 D. T. Seaton, S. Schnabel, M. Bachmann and D. P. Landau, *Int. J. Mod. Phys. C*, 2012, **23**, 1240004; D. T. Seaton, S. Schnabel, D. P. Landau and M. Bachmann, *Phys. Rev. Lett.*, 2013, **110**, 028103.

87 M. Marenz and W. Janke, *Knots as topological order parameter for semi-flexible polymers*, 2015, e-print arXiv:1506.07376 [cond-mat.soft].

88 Z. Wang and X. He, *J. Chem. Phys.*, 2011, **135**, 094902.

89 Z. Wang, L. Wang, Y. Chen and X. He, *Soft Matter*, 2014, **10**, 4142–4150.

90 S. Schöbl, J. Zierenberg and W. Janke, *Phys. Rev. E: Stat., Nonlinear, Soft Matter Phys.*, 2011, **84**, 051805.

91 S. Schöbl, J. Zierenberg and W. Janke, *J. Phys. A: Math. Theor.*, 2012, **45**, 475002.

92 T. Garel and H. Orland, *J. Phys. A: Math. Gen.*, 1990, **23**, L621–L626.

93 S. Schöbl, S. Sturm, W. Janke and K. Kroy, *Phys. Rev. Lett.*, 2014, **113**, 238302.

94 N. Urakami and M. Takasu, *Mol. Simul.*, 1997, **19**, 63–73.

95 Y. U. Wang, H. N. Chen and J. J. Liang, *J. Chem. Phys.*, 2001, **115**, 3951–3956.

96 T. Koga, *Eur. Phys. J. E: Soft Matter Biol. Phys.*, 2005, **17**, 381–388.

97 Z. Wang, L. Wang and X. He, *Soft Matter*, 2013, **9**, 3106–3116.

98 E. N. Govorun, V. A. Ivanov, A. R. Khokhlov, P. G. Khalatur, A. L. Bovorinsky and A. Y. Grosberg, *Phys. Rev. E: Stat., Nonlinear, Soft Matter Phys.*, 2001, **64**, 040903(R).

99 M. Bachmann and W. Janke, *J. Chem. Phys.*, 2004, **120**, 6779–6791.

100 M. Bachmann, H. Arkın and W. Janke, *Phys. Rev. E: Stat., Nonlinear, Soft Matter Phys.*, 2005, **71**, 031906.

101 Y. W. Li, T. Wüst and D. P. Landau, *Comput. Phys. Commun.*, 2011, **182**, 1896–1899.

102 T. Wüst and D. P. Landau, *J. Chem. Phys.*, 2012, **137**, 064903.

103 J. F. Liu, B. B. Song, Y. L. Yao, Y. Xue, W. J. Liu and Z. X. Liu, *Phys. Rev. E: Stat., Nonlinear, Soft Matter Phys.*, 2014, **90**, 042715.

104 T. Wüst, D. Reith and P. Virnau, *Phys. Rev. Lett.*, 2015, **114**, 028102.

105 A. Kallias, M. Bachmann and W. Janke, *J. Chem. Phys.*, 2008, **128**, 055102; A. Böker and W. Paul, *Wang-Landau simulation of Go model molecules*, preprint.

106 G. J. Shi, T. Vogel, T. Wüst, Y. W. Li and D. P. Landau, *Phys. Rev. E: Stat., Nonlinear, Soft Matter Phys.*, 2014, **90**, 033307.

107 Y. Yoshida and Y. Hiwatari, *Mol. Simul.*, 1999, **22**, 91–121.

108 M. Bachmann and W. Janke, *Phys. Rev. Lett.*, 2005, **95**, 058102.

109 M. Möddel, M. Bachmann and W. Janke, *J. Phys. Chem. B*, 2009, **113**, 3314–3323; M. Möddel, W. Janke and M. Bachmann, *Phys. Chem. Chem. Phys.*, 2010, **12**, 11548–11554; M. Möddel, W. Janke and M. Bachmann, *Comput. Phys. Commun.*, 2011, **182**, 1961–1965.

110 T. Chen, L. Wang, X. Liu and H. Liang, *J. Chem. Phys.*, 2009, **130**, 244905.

111 N. A. Volkov, P. N. Vorontsov-Velyaminov and A. P. Lyubartsev, *Macromol. Theory Simul.*, 2011, **20**, 496–509.

112 J. Luettmer-Strathmann, F. Rampf, W. Paul and K. Binder, *J. Chem. Phys.*, 2008, **128**, 064903; J. Luettmer-Strathmann and K. Binder, *J. Chem. Phys.*, 2014, **141**, 114911.

113 M. P. Taylor and J. Luettmer-Strathmann, *J. Chem. Phys.*, 2014, **141**, 204906.

114 V. A. Ivanov, J. A. Martemyanova, M. Müller, W. Paul and K. Binder, *J. Phys. Chem. B*, 2009, **113**, 3653–3668.

115 M. Möddel, W. Janke and M. Bachmann, *Macromolecules*, 2011, **44**, 9013–9019.

116 T. Chen, L. Wang, X. Lin, Y. Liu and H. Liang, *J. Chem. Phys.*, 2009, **130**, 244905.

117 L. Wang, T. Chen, X. Lin, Y. Liu and H. Liang, *J. Chem. Phys.*, 2009, **131**, 244902.

118 H. Arkın and W. Janke, *Phys. Rev. E: Stat., Nonlinear, Soft Matter Phys.*, 2012, **85**, 051802; H. Arkın and W. Janke, *J. Phys. Chem. B*, 2012, **116**, 10379–10386; H. Arkın and W. Janke, *J. Chem. Phys.*, 2013, **138**, 054904.

119 H. Arkın and W. Janke, *Eur. Phys. J.: Spec. Top.*, 2013, **216**, 181–190.

120 M. Möddel, W. Janke and M. Bachmann, *Phys. Rev. Lett.*, 2014, **112**, 148303.

121 S. Karalus, W. Janke and M. Bachmann, *Phys. Rev. Lett.*, 2011, **84**, 031803.

122 C. Junghans, M. Bachmann and W. Janke, *J. Chem. Phys.*, 2008, **128**, 085103.

123 C. Junghans, W. Janke and M. Bachmann, *Comput. Phys. Commun.*, 2011, **182**, 1937–1940.

124 T. Chen, X. Lin, Y. Liu and H. Liang, *Phys. Rev. E: Stat., Nonlinear, Soft Matter Phys.*, 2007, **76**, 045110.

125 R. B. Frigori, L. G. Rizzi and N. A. Alves, *J. Chem. Phys.*, 2013, **138**, 015102.

126 C. Junghans, M. Bachmann and W. Janke, *Europhys. Lett.*, 2009, **87**, 40002.

127 T. Chen, X. Lin, Y. Liu, T. Lu and H. Liang, *Phys. Rev. E: Stat., Nonlinear, Soft Matter Phys.*, 2008, **78**, 056101.

128 J. Zierenberg, M. Mueller, P. Schierz, M. Marenz and W. Janke, *J. Chem. Phys.*, 2014, **141**, 114908.

129 A. Nußbaumer, E. Bittner and W. Janke, *Phys. Rev. E: Stat., Nonlinear, Soft Matter Phys.*, 2008, **77**, 041109.

130 J. Zierenberg and W. Janke, *Phys. Rev. E: Stat., Nonlinear, Soft Matter Phys.*, 2015, **92**, 012134.

131 J. Zierenberg and W. Janke, *Europhys. Lett.*, 2015, **109**, 28002.

132 S. Kumar and A. Z. Panagiotopoulos, *Phys. Rev. Lett.*, 1999, **82**, 5060–5063.

133 T. Shakirov and W. Paul, *What drives crystallization in melts of semi-flexible polymers? A Wang-Landau type Monte Carlo study*, preprint.